Geophysical Research Letters

RESEARCH LETTER
10.1029/2024GL113668

Diverse Timing of El Niño Onset Linked to Preconditioned Recharge State and Occurrence of Westerly Wind Bursts

Yu Liu[1], Wenjun Zhang[1], Feng Jiang[2], Han-Ching Chen[1], Fei-Fei Jin[3], and Suqiong Hu[4]

[1]CIC-FEMD/KLME, State Key Laboratory of Climate System Prediction and Risk Management, Nanjing University of Information Science and Technology, Nanjing, China, [2]Lamont-Doherty Earth Observatory, Columbia University, Palisades, NY, USA, [3]Department of Atmospheric Sciences, School of Ocean and Earth Science and Technology, University of Hawai'i at Manoa, Honolulu, HI, USA, [4]Nicholas School of the Environment, Duke University, Durham, NC, USA

Key Points:

- El Niño exhibits considerable variation in its onset timing, ranging from March to September
- The onset of El Niño is closely linked to the preconditioned oceanic recharge state and the occurrence of westerly wind bursts
- MIROC6 simulations and a conceptual model support the curial roles of recharge conditions and WWBs in determining El Niño onset timing

Supporting Information:

Supporting Information may be found in the online version of this article.

Correspondence to:

W. Zhang,
zhangwj@nuist.edu.cn

Citation:

Liu, Y., Zhang, W., Jiang, F., Chen, H.-C., Jin, F.-F., & Hu, S. (2025). Diverse timing of El Niño onset linked to preconditioned recharge state and occurrence of westerly wind bursts. *Geophysical Research Letters*, *52*, e2024GL113668. https://doi.org/10.1029/2024GL113668

Received 15 NOV 2024
Accepted 1 MAR 2025

Abstract El Niño is generally phase-locked to the boreal winter but displays significant variability in its onset timing, contributing to its diverse climate impacts. The physical mechanisms driving this variability remain inadequately understood. This study demonstrates that onset of El Niño events can occur over a broad range of months from March to September, with its onset timing closely linked to the precondition of oceanic recharged state and the occurrence of westerly wind bursts (WWBs) in the preceding spring. A stronger recharged state and increased frequency of WWBs promote earlier onset by efficiently transporting warm water to the equatorial eastern Pacific. Supporting evidence from MIROC6 simulations and a conceptual model underscores the crucial roles of both the recharged state and WWBs in determining the timing of El Niño onset. These results enhance our understanding of El Niño dynamics and hold important implications for seasonal climate prediction.

Plain Language Summary El Niño, a significant climate phenomenon, arises from interactions between the ocean and atmosphere in the tropical Pacific, profoundly affecting global weather patterns. Currently, predicting the precise timing of the El Niño onset remains a scientific challenge. In this study, we find that the onset of El Niño varies considerably, ranging from March to September. This variability is strongly linked to the precondition of oceanic heat buildup (recharged state) and the occurrence of westerly wind bursts (WWBs). A stronger recharged state and increased frequency of WWBs in the preceding spring can lead to an earlier El Niño onset by accelerating the eastward movement of warm water toward the central-eastern equatorial Pacific. These findings deepen our understanding of El Niño dynamics and offers valuable insights for improving seasonal climate predictions.

1. Introduction

The El Niño–Southern Oscillation (ENSO) is the most significant source of interannual climate variability, originating from large-scale coupled interactions between the ocean and atmosphere in the tropical Pacific. ENSO has received significant scientific attention due to its far-reaching impacts on global climate (McPhaden et al., 2006; Timmermann et al., 2018; Wallace et al., 1998). The rapid growth of ENSO events is largely attributed to positive ocean-atmosphere feedback, known as the Bjerknes feedback, in the equatorial Pacific, where a weakening of the zonal sea surface temperature (SST) gradient drives westerly wind anomalies, further reducing the SST gradient and amplifying the system (Bjerknes, 1969). Over the past several decades, various mechanisms have been proposed to understand ENSO's phase transition between its warm and cold phases, providing the theoretical basis for understanding ENSO dynamics and its predictability (e.g., Battisti & Hirst, 1989; Jin, 1997; Suarez et al., 1988; Wyrtki, 1975).

The warm phase of ENSO, El Niño, is typically phase-locked to the local seasonal cycle (H. C. Chen & Jin, 2020), with its development starting in boreal spring or summer, peaking in boreal winter, and decaying in the subsequent seasons. However, the onset timing of El Niño varies considerably, occurring between boreal spring and autumn (Horii & Hanawa, 2004; Lee et al., 2014; Wu et al., 2021; Xu & Chan, 2001). This variability in onset timing can lead to different global climate responses (Cai et al., 2019; Lopez et al., 2022; Jiang et al., 2023). For example, early-onset El Niño events can drive cooling in the eastern tropical Atlantic, a response less pronounced in late-onset events (Jiang et al., 2023). Despite the importance of El Niño onset timing, the underlying physical mechanisms driving this variability remain inadequately understood.

The upper ocean heat content (OHC) is a valuable precursor for ENSO SST development, as the accumulation of the warm water usually leads SST variations by several months (McPhaden et al., 2006; Meinen & McPhaden, 2000; Zhang et al., 2019). Previous studies have shown that El Niño events can be predicted 6–9 months in advance, primarily due to the slow exchange of OHC between the equatorial and off-equatorial Pacific Ocean (Cane & Zebiak, 1985; Wyrtki, 1985; Zebiak, 1989). The charge and discharge process of ocean heat content involves complex interactions between the atmosphere and the ocean. This dynamic is encapsulated in the recharge oscillator theory (Jin, 1997), which describes how SST and oceanic adjustment to surface wind changes governs the oscillatory behavior of El Niño. Additionally, westerly wind bursts (WWBs), a major disruption to the prevailing easterly trade winds in the equatorial Pacific (Harrison & Giese, 1991), play a substantial role in triggering El Niño onset by generating eastward-propagating downwelling Kelvin waves that deepen the thermocline in the central-eastern equatorial Pacific (e.g., Boulanger et al., 2001; Fedorov et al., 2015; Lengaigne et al., 2004; McPhaden & Yu, 1999; Xuan et al., 2022). A suppressed thermocline further promotes the warming of SST via climatological upwelling, and this process is so-called thermocline feedback (Jin & An, 1999).

Given the significance of both ocean heat buildup and WWBs in the development of ENSO, it is compelling to hypothesize that these oceanic and atmospheric conditions are the key factors influencing the timing of El Niño onset. In this study, we investigate the variability in El Niño onset timing and examine its connection to oceanic and atmospheric preconditions in the tropical Pacific. Our findings demonstrate that the timing of El Niño onset is closely linked to the precondition of oceanic recharged state (i.e., warm water buildup) and the frequency of WWBs in the preceding spring.

2. Data and Method

2.1. Observational and Climate Model Data

The SST data utilized in this study are derived from the National Oceanic and Atmospheric Administration (NOAA) high-resolution blended analysis of Optimum Interpolation SST version 2 (OISSTv2), providing monthly SST data with a spatial resolution of 2.0° × 2.0° (Reynolds et al., 2007). The daily 10-m wind data, with a spatial resolution of 0.5° × 0.5°, are sourced from the European Center for Medium-Range Weather Forecasts (ECMWF) Reanalysis Version 5 dataset (ERA5) (Hersbach et al., 2020). The upper OHC index is obtained from the Tropical Atmosphere Ocean/Pacific Marine Environmental Laboratory (TAO/PMEL). The OHC is defined as the anomalous ocean temperature averaged between 0 and 300 m in depth within the equatorial Pacific region (5°S–5°N, 120°E–80°W), representing the upper Pacific ocean's heat recharge state. Monthly data for the 20°C isotherm depth and potential temperature are derived from the ECMWF Ocean Reanalysis System 5 (ORAS5), with a spatial resolution of 1.0° × 1.0° (Zuo et al., 2019). Daily outgoing longwave flux (OLR) data is derived from NOAA interpolated OLR data provided by NOAA Physical Sciences Laboratory (PSL) with a spatial resolution of 2° × 2° (Liebmann & Smith, 1996). The study covers the period from 1980 to 2020, with anomalies calculated relative to the climatological mean over the entire period. To validate the main conclusions based on the observations, we incorporate the output from the Model for Interdisciplinary Research on Climate version 6 (MIROC6) pre-industrial control (pi-control) simulation (Tatebe et al., 2019). Here, one ensemble member (r1i1p1f1) is analyzed by using the last 150 years of pi-control simulations. Anomalies in the model simulation are calculated as departures from the model's climatology over the full study period.

2.2. Definition of El Niño Onset Timing and Westerly Wind Bursts

According to the definition from Climate Prediction Center (CPC), El Niño is identified when 3-month running mean of the Niño3.4 SST anomaly (5°S–5°N, 120°–170°W) exceeds the threshold of 0.5°C for at least five consecutive months. Based on this definition, 11 El Niño developing years are identified (1982, 1986, 1991, 1994, 1997, 2002, 2004, 2006, 2009, 2014, and 2018) from 1980 to 2020. Given the variation in the zonal location of the El Niño onset, it is necessary to consider El Niño indices across different regions of the equatorial Pacific. Therefore, the onset of El Niño is defined when the area-averaged SST anomalies in any of the Niño4 (5°S–5°N, 160°E–150°W), Niño3.4 (5°S–5°N, 170°W–120°W), or Niño3 (5°S–5°N, 150°W–90°W) regions surpass 0.5 standard deviations.

WWBs are detected based on the definition proposed by Harrison and Vecchi (1997) and Xuan et al. (2024), using the daily 10-m zonal wind anomalies. Firstly, the raw wind data is interpolated onto a 1-degree latitude by 10-degree longitude grid using the bilinear interpolation method. A 90-day high-pass filter is applied to the data to

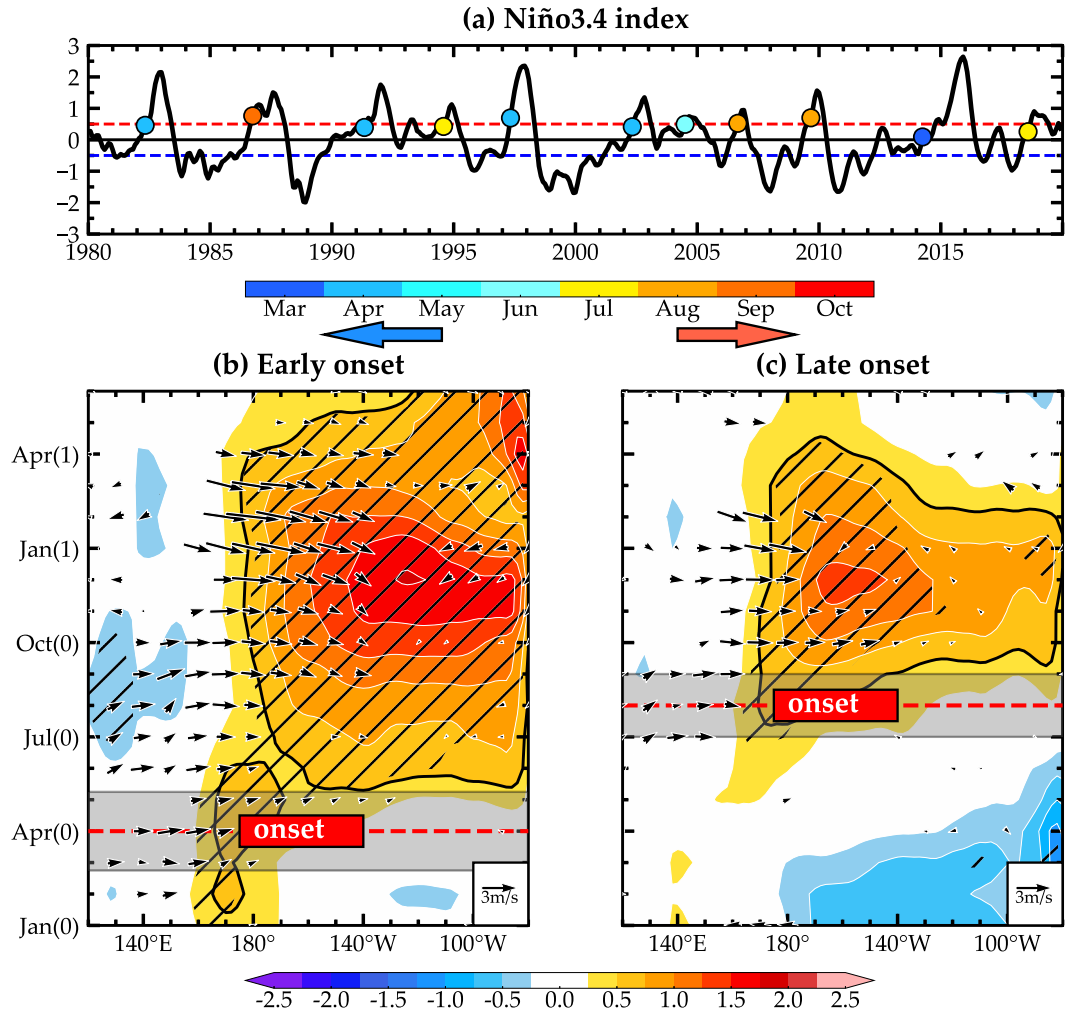

Figure 1. (a) Time-series of the Niño3.4 index during the period of 1980–2020, with colored dots indicating the onset month of El Niño events. (b) Hovmöller diagrams for the composite evolution of SST (shading; °C) and zonal 10-m wind (vector; m/s) anomalies in the equatorial Pacific (5°S–5°N) during early-onset El Niño events. (c) Same as (b), but for late-onset El Niño events. In (b) and (c), the red lines represent the mean onset timing of El Niño, with gray shading indicating one standard deviation. The black thick contours correspond to the 0.5°C isotherm of SST anomalies and black hatching indicates values that exceed the 95% significance level. Wind anomalies are shown only when they are significant at the 95% confidence level. The arrows denote the two groups of El Niño with different onset timing (blue, early-onset events; orange, late-onset events).

remove possible influences of the low-frequency variability. WWBs are then identified at grid points where zonal wind anomalies exceed 5 m/s and persist for at least three consecutive days. This method captures the basic features of WWBs, focusing on their zonal extension, duration and magnitude, similar to previous studies (e.g., Chiodi et al., 2014; Hartten, 1996; Seiki & Takayabu, 2007). In this study, we calculate the frequency of WWBs (days per month) and WWB accumulated strength (time integration of zonal wind anomalies associated with WWBs) over the equatorial Pacific (5°S–5°N, 120°E−120°W) to characterize WWBs activity. The quantitative conclusions of our analysis remain consistent when using WWB frequency or strength. Therefore, we only show the results based on WWB frequency in this study.

3. Results

Figure 1a shows the time series of the Niño3.4 index over the period of 1980–2020, with the onset month of El Niño marked by colored circles. The onset timing of El Niño displays considerable event-to-event variations, ranging from March to September. To examine possible differences in the associated oceanic and atmospheric

conditions, the El Niño events are categorized into two groups: early-onset (onset before June) and late-onset (onset after June). The averaged onset month of early-onset events is around April, while for late-onset events it is approximately August. The evolution of SST and related surface wind anomalies differs significantly between early- and late-onset El Niño events during their development phases. As shown in Figure 1b, early-onset El Niño events are characterized by pronounced warm SST anomalies in the western-central equatorial Pacific during the preceding spring season, accompanied with substantial westerly wind anomalies in the western Pacific. These initial warm SST anomalies then amplify rapidly, evolving into a large-scale warming pattern with strong intensity in the central-eastern tropical pacific over the following months. In contrast, late-onset El Niño events experience negative SST anomalies in the central-eastern equatorial Pacific during spring, with marginally significant cooling near the South American coast (Figure 1c). Positive SST anomalies and corresponding westerly anomalies are not remarkably detected until July, after which the SST anomalies develop fast via the positive ocean-atmosphere feedback based on the Bjerknes mechanism. It is important to note that super El Niño events are typically characterized by the early-onset timings and large-scale SST anomalies across the equatorial Pacific. However, these results do not support a direct physical link between El Niño onset timing and its spatial structure diversity. For example, some central Pacific (CP) El Niño events can develop rapidly with early onset, while some eastern Pacific (EP) El Niño events may exhibit late-onset features in observations.

Based on the recharge oscillator theory (Jin, 1997; Meinen & McPhaden, 2000), the precondition of oceanic recharged state (i.e., the buildup of subsurface warm water), plays a crucial role in the subsequent development of El Niño events. In particular, the oceanic recharge state around February has been closely linked to the amplitude of the ensuing El Niño (e.g., Lai et al., 2015; McPhaden, 1999; McPhaden et al., 2006; Xuan et al., 2022). To investigate the potential relationship between the Pacific oceanic recharge state and the timing of El Niño onset, the temporal evolution of OHC anomalies during early- and late-onset El Niño events is displayed in Figure 2a. The basin-wide OHC for early-onset El Niño events is significantly positive during the early spring, while the OHC for late-onset El Niño events is near-zero (Figure 2a). As shown in Figure 2c, early-onset El Niño events are generally preceded by a pronounced buildup of warm water in the equatorial Pacific during their developing spring. In contrast, late-onset events are characterized with a dipole-like subsurface temperature across the equatorial Pacific (Figure 2d). This is closely related to the fact that late-onset events generally exhibit a transition from a Pacific cooling with a weak recharge of OHC in the previous winter (Figure S1b in Supporting Information S1). For early-onset events, however, a pronounced recharge of OHC can be detected in the western equatorial Pacific prior to the developing spring (Figure S1a in Supporting Information S1). Accordingly, early-onset events are usually characterized by substantial SST warming in the equatorial western-central Pacific and a basin-wide accumulation of warm water during spring of the developing year (Figure 2c). The OHC is higher on average in early-onset El Niño events relative to late-onset events as they approach the peak winter, with the difference diminishing until it becomes statistically indistinguishable. As shown in Figure 3a, the El Niño onset timing and spring (Feb-March-April, FMA) OHC anomalies (Figure 3a) show a significant negative correlation ($r = -0.68$, statistically significant at the 95% confidence level).

Previous studies have also proposed that WWBs contribute to the irregularity of El Niño development (e.g., Chen et al., 2015; Fedorov et al., 2015; Lengaigne et al., 2003). Our analysis is extended by comparing the frequency of WWBs between early- and late-onset El Niño events. The results display a clear distinction in the frequency of WWBs during spring of the developing year. As shown in Figure 2b, early-onset events exhibit frequent WWB during this period, with more occurrence spanning a broad region of the western Pacific north of equator from 130°E to 170°E (Figure 2c). In contrast, the WWB activity is suppressed for late-onset events (Figure 2b), which is confined to a small region near 140°E (Figure 2d). Earlier studies often considered WWBs as a stochastic forcing, independent from El Niño events (e.g., Kleeman & Moore, 1997). However, recent studies argued that WWBs may be modulated by various physical processes (McPhaden, 1999; Lengaigne et al., 2003; Seiki & Takayabu, 2007; Tziperman & Yu, 2007; Xuan et al., 2024). Our analysis reveals that the occurrence of frequent WWBs is linked to local SST anomalies and deep atmospheric convection over the western-central Pacific (Figure S2 in Supporting Information S1). These WWBs, in turn, could facilitate the onset of El Niño. This relationship is evident in the scatterplot of WWB frequency and El Niño onset timing (Figure 3b), which exhibits a similar negative relationship ($r = -0.74$, statistically significant at the 95% confidence level). We further assess the combined influence of OHC and WWB conditions by reconstructing the onset timing of El Niño using multiple-variable linear regression based on spring OHC and WWB frequency (Figure 3c). The reconstructed onset timing is highly correlated with the observed onset timing ($R = 0.81$, statistically significant at the 95%

10.1029/2024GL113668

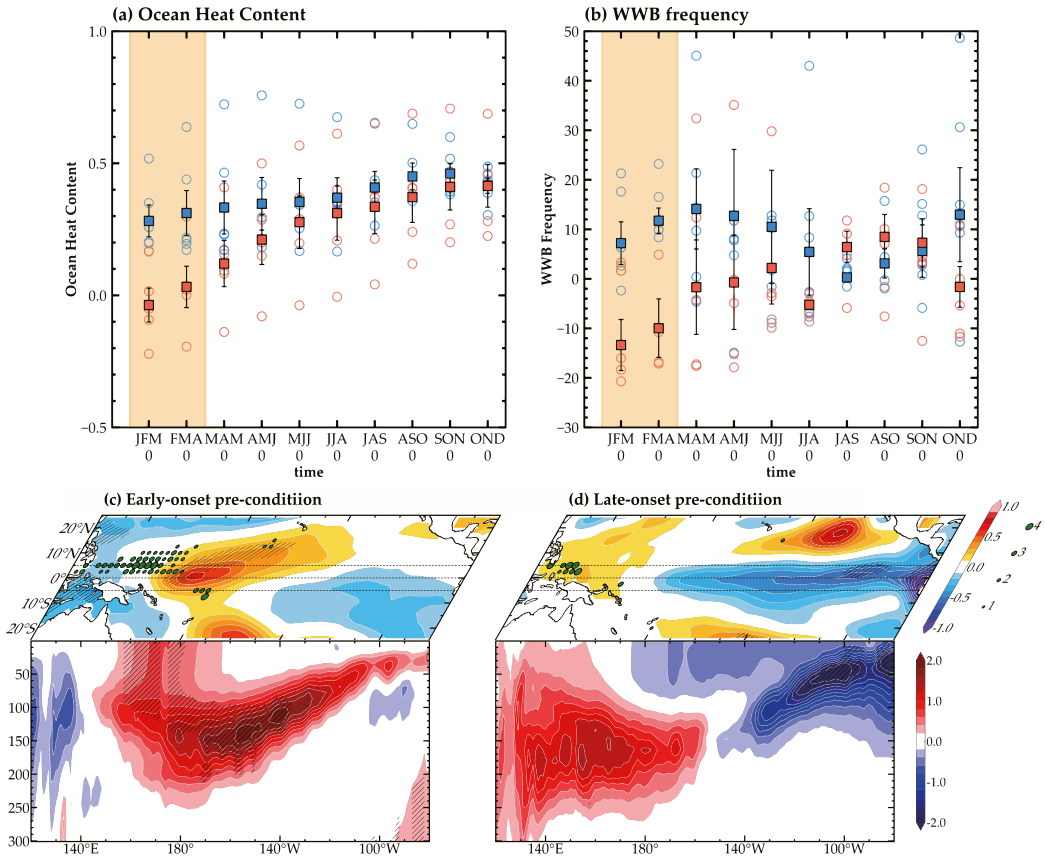

Figure 2. (a) Composite time evolution of equatorial Pacific (5°S–5°N, 120°E−80°W) OHC (°C) anomalies during early-onset (blue bars/circles) and late-onset (orange bars/circles) El Niño events. Bars denote the composite mean and circles indicate values for individual events. Black error bars represent one standard deviation, and yellow shading denotes differences between early- and late-onset composites that are significant at the 95% level. (b) Same as (a), but for the WWB frequency anomalies. (c) Composite three-dimensional distribution of SST (shading; °C), WWB frequency (green dots; days per month) and equatorially averaged (5°S–5°N) subsurface temperature (shading; °C) anomalies during the boreal spring [FMA(0)] for early-onset El Niño events. Black hatching indicates composite values that exceed the 95% significance level. WWB frequency is shown only when they are significant at the 95% confidence level. (d) Same as (c), but for late-onset events.

confidence level), suggesting that the variations of the El Niño onset timing can be largely explained by the preceding spring OHC and WWB conditions. Besides, we calculate the partial correlation of the two variables with El Niño onset timing to examine their relative contributions. The partial correlation coefficient for WWBs is −0.6, which is higher than −0.48 for OHC. This result indicates that WWBs may play a stronger role in determining the onset timing of El Niño.

Due to the limited sample size in observations, the outputs from the MIROC6 pi-control experiment are further utilized to examine the relationship between El Niño onset timing and preceding OHC and WWB activity. The model is capable of realistically simulating the fundamental features of El Niño including the oceanic recharge process and WWB activity (Tatebe et al., 2019). In this simulation, 23 El Niño events are identified, classifying 13 as early-onset and 10 as late-onset, following the same criteria as the observational analyses. The MIROC6 model successfully captures the general evolution of SST and wind patterns associated with both groups of El Niño, though with some discrepancies (Figure S3 in Supporting Information S1). Early-onset El Niño events are preceded by SST warming in the western Pacific, similar to the observation but with reduced intensity and a more westward extension (Figure S3a in Supporting Information S1). In contrast, late-onset events are marked by a transition from a cooling state in the Pacific, consistent with the observation (Figure S3b in Supporting Information S1). It is noted that both groups of El Niño show an earlier occurrence in the central-eastern equatorial Pacific in the model compared to observations, leading by about 1 month. Moreover, the MIROC6 model shows a

10.1029/2024GL113668

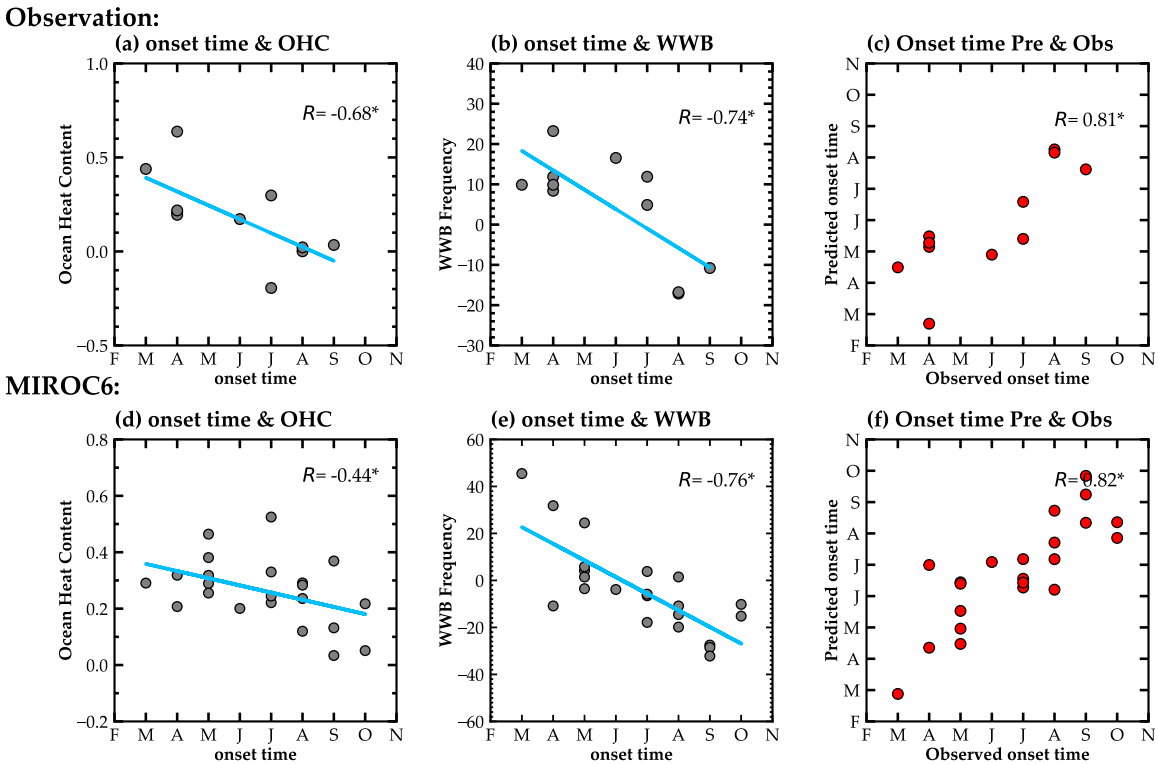

Figure 3. Scatterplots of observed onset timing of El Niño against (a) spring (FMA) OHC anomalies, (b) spring WWB frequency anomalies and (c) reconstructed onset timing using a linear fit based on spring OHC and WWB frequency anomalies (blue lines), with correlation coefficients (R) indicated. The symbol "*" denotes the correlation coefficients that are significant at the 95% confidence level. (d)–(f) Same as (a)–(c), but for outputs from the MIROC6 simulation during January-February-March (JFM).

strong connection between El Niño onset timing and anomalies in OHC and WWB frequency during the preceding spring (Figure S4 in Supporting Information S1). This is supported by scatterplot analyses (Figures 3d and 3e), showing significant correlation between onset timing and both OHC ($R = -0.44$) and WWB frequency ($r = -0.76$), with both correlations exceeding the 95% confidence level. The combination of the OHC (with partial coefficient as high as 0.46) and WWB (with partial coefficient as high as 0.76) conditions account for approximately 67% of the variability in simulated onset timing of El Niño (Figure 3f). These findings from the MIROC6 model validate the observational results, indicating that stronger warm water buildup and more frequent WWBs favor earlier onset of El Niño events.

We next adapt the extended recharged oscillator (RO) model (see Text S1 in Supporting Information S1) to perform a series of sensitive experiments aimed at elucidating the critical roles of spring OHC and WWBs in determining the timing of El Niño onset. Four ensembles of experiments are performed, varying initial ocean heat recharge and wind forcing during spring within the RO model (Exp1_NoW, Exp1_W, Exp2_NoW, and Exp2_W; see Table S1 in Supporting information S1). All experiments are initialized with zero SST anomalies. In the first ensemble (Exp1_NoW), the initial oceanic recharge state, represented by equatorial thermocline depth anomalies, is set to 6 m (about 0.5 times standard deviation of observed thermocline depth anomalies during developing spring of El Niño), with wind forcing randomized. In the second ensemble (Exp1_W), several WWBs are superimposed during spring of developing year, while maintaining the initial oceanic recharge at 6 m to assess WWB impacts. The third (Exp2_NoW) and fourth (Exp2_W) ensembles initialize the oceanic recharge at 12 m (approximating to observed thermocline depth anomalies during FMA of the 1997 El Niño), reflecting a stronger precondition of ocean heat recharge. In Exp2_NoW, wind forcing is randomized, whereas in Exp2_W, the wind forcing is configured to simulate the occurrence of WWBs.

In the experiments with weak initial ocean heat recharge, the evolution of El Niño SST anomalies, in the absence of imposed westerly wind forcing, follows a regular El Niño progression with onset occurring during June on average (Figure 4a). When the westerly wind forcing is applied to these weakly charged ensembles, the SST

10.1029/2024GL113668

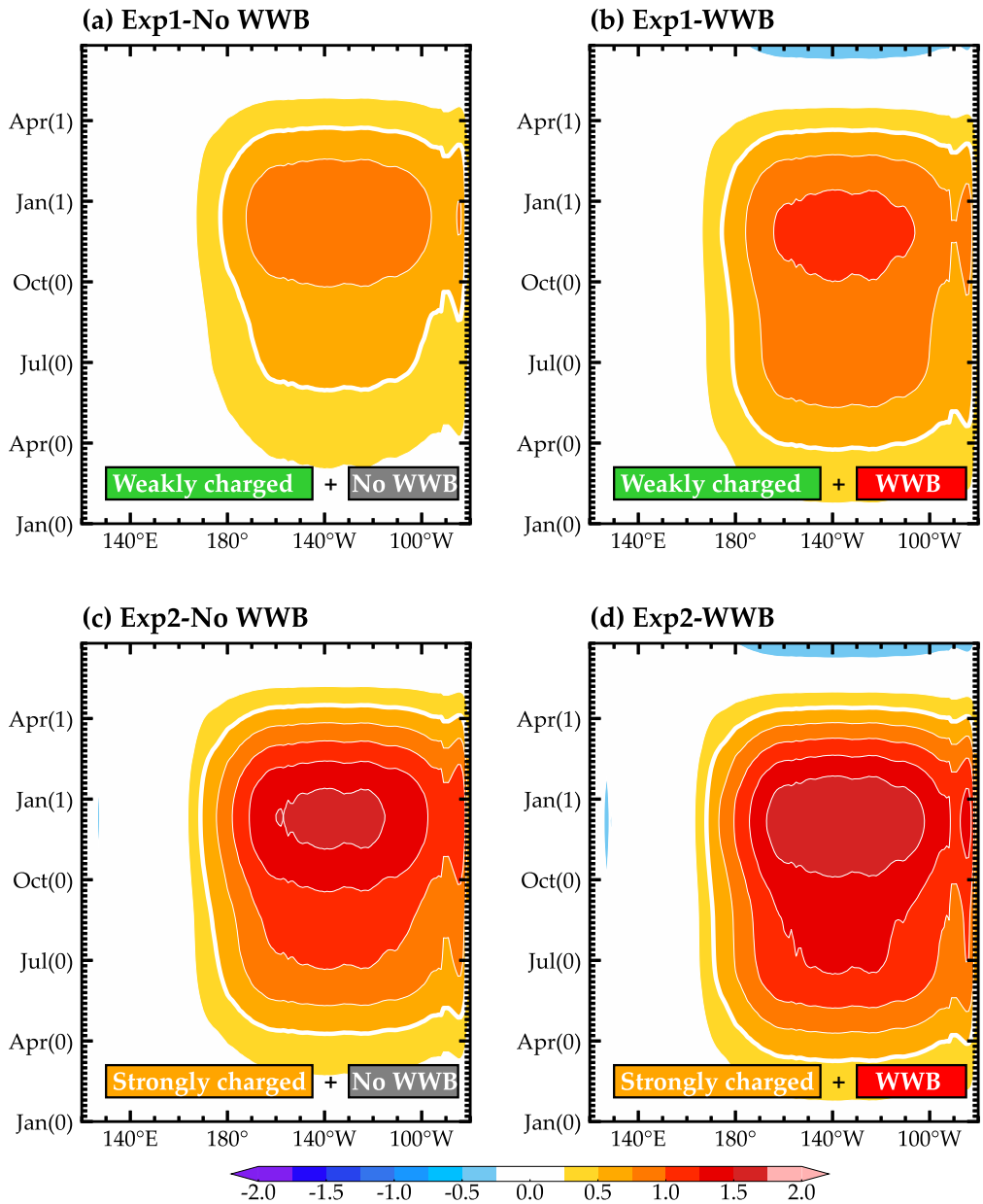

Figure 4. Hovmöller diagrams for the evolution of SST (shading; °C) anomalies at the equatorial Pacific (5°S–5°N) for weakly charged sets without imposed WWB (a) and with imposed WWB (b). (c) and (d) are same as upper two panels, but for the strongly charged sets. White thick contours represent the 0.5°C isotherm of the SST anomalies.

anomalies associated with El Niño develop more rapidly, with the onset occurring earlier, around April (Figure 4b). In the experiments with enhanced initial heat recharge, the SST anomalies grow more quickly, with increased intensity and an earlier onset (Figure 4c). Correspondingly, the application of WWB forcing in these strongly recharged ensembles further accelerates the growth rate of El Niño and facilitates an even earlier onset (Figure 4d). These sensitivity experiments based on the conceptual model, support the observational and MIROC6 results, highlighting the importance of oceanic recharge state and WWB activity in determining the timing of El Niño onset.

4. Conclusions and Discussion

In the present study, we show that the El Niño onset timing exhibits considerable variability, with onset months ranging from March to September. The onset timing is demonstrated to be closely associated with the warm water buildup and WWB activity in the equatorial Pacific during the preceding spring season. Early-onset El Niño events, typically emerging around April, are usually characterized by a pronounced buildup of warm water and frequent WWB occurrence during spring of the developing year. The frequent WWBs can effectively transport the warm water eastward, fostering the development of SST anomalies, and thus accelerating the onset of El Niño. In contrast, late-onset events, which tend to emerge around August, are preceded by a weak recharge of oceanic heat in the equatorial with weak WWB activity. The weak recharge state and less frequent WWBs are insufficient to drive the eastward extension of warm water, delaying the El Niño onset. Our findings are further supported by simulations from the MIROC6 model and a conceptual RO model. This study provides a dynamical understanding of El Niño onset timing by focusing on the role of warm water buildup and WWB activity, thereby enhancing our ability to predict the diversity in El Niño events, particularly with regard to their onset timing.

The warm water in the upper Pacific Ocean evolves gradually in response to surface wind variations via the recharge-discharge processes. Compared to the slow oceanic changes, atmospheric variability exhibits a high-frequency behavior, which remains less thoroughly understood. Our analysis reveals that the WWB activity appears to be closely associated with SST anomalies in the equatorial western-central Pacific, a region situated near the eastern edge of the warm pool (Figure 2c and Figure S2a in Supporting Information S1). This region is highly sensitive to SST fluctuations, where even small anomalies can excite substantial atmospheric convective responses due to the high background SST (Barsugli & Sardeshmukh, 2002; Graham & Barnett, 1987; Hu et al., 2024; Palmer & Mansfield, 1984). The SST anomaly patterns in the western-central Pacific exhibit a significant difference between early-onset and late-onset events, despite both displaying positive subsurface temperature anomalies near the thermocline layer (~150 m) (Figures 2c and 2d). In late-onset events, the thermal structure in the western-central equatorial Pacific is characterized by a cooler surface and warmer subsurface. The cooling SST anomalies and corresponding easterly wind anomalies inhibit occurrence of WWBs. In contrast, in early-onset events, warming from subsurface to surface layers in the western-central tropical Pacific facilitates more frequent WWBs by enhancing deep atmospheric convection (Lengaigne et al., 2004). This warming during boreal spring is proposed as a potential precursor for the development of super El Niño (Kim & An, 2018). However, the dynamics behind this SST warming is complicated; for example, the conventional relationship between sea level and thermocline depth is not evident in the central Pacific (Zhao et al., 2021). Other studies suggests that nonlinear oceanic processes, such as ocean mixing, could play a non-negligible role in SST variations (Dewitte et al., 2009; Yuan et al., 2020). Furthermore, frequent WWBs can amplify SST warming in the western-central tropical Pacific by expanding the warm pool eastward. While we argue that frequent WWBs in early spring contribute to the early onset of El Niño events, the question of whether SST anomalies predominantly drive WWB activity or if WWBs initiate these SST warming remains an open question that deserves future investigation.

Data Availability Statement

The SST data sets from the OISSTv2 are provided by NOAA at https://www.psl.noaa.gov/data/gridded/data.noaa.oisst.v2.html (Reynolds et al., 2007) is used in this paper. The 10-m wind data is obtained from the ERA5 produced by ECMWF (Hersbach et al., 2023). The OHC index is derived from TAO/PMEL at https://www.pmel.noaa.gov/tao/wwv/data/. The ocean temperature and D20 can be obtained from ECMWF ORAS5 (Copernicus Climate Change Service, Climate Data Store, 2021). The OLR data is derived from NOAA interpolated OLR data provided by the NOAA PSL at https://www.psl.noaa.gov/data/gridded/data.olrcdr.interp.html (Liebmann & Smith, 1996). The MIROC6 model outputs can be accessed at https://esgf-node.llnl.gov/projects/cmip6/.

Acknowledgments
This work was supported by the National Nature Science Foundation of China (42088101, 42125501).

References

Barsugli, J. J., & Sardeshmukh, P. D. (2002). Global atmospheric sensitivity to tropical SST anomalies throughout the Indo-Pacific basin. *Journal of Climate*, *15*(23), 3427–3442. https://doi.org/10.1175/1520-0442(2002)015<3427:gastts>2.0.co;2

Battisti, D. S., & Hirst, A. C. (1989). Interannual variability in a tropical atmosphere–ocean model: Influence of the basic state, ocean geometry and nonlinearity. *Journal of the Atmospheric Sciences*, *46*(12), 1687–1712. https://doi.org/10.1175/1520-0469(1989)046<1687:iviata>2.0.co;2

Bjerknes, J. (1969). Atmospheric teleconnections from the equatorial Pacific. *Monthly Weather Review*, *97*(3), 163–172. https://doi.org/10.1175/1520-0493(1969)097<0163:atftep>2.3.co;2

Boulanger, J. P., Durand, E., Duvel, J. P., Menkès, C., Delécluse, P., Imbard, M., et al. (2001). Role of non-linear oceanic processes in the response to westerly wind events: New implications for the 1997 El Niño onset. *Geophysical Research Letters*, *28*(8), 1603–1606. https://doi.org/10.1029/2000gl012364

Cai, J., Xu, J., Guan, Z., & Powell, A. M. (2019). Interdecadal variability of El Niño onset and its impact on monsoon systems over areas encircling the Pacific Ocean. *Climate Dynamics*, *52*(12), 7173–7188. https://doi.org/10.1007/s00382-016-3377-z

Cane, M. A., & Zebiak, S. E. (1985). A theory for El Niño and the southern oscillation. *Science*, *228*(4703), 1085–1087. https://doi.org/10.1126/science.228.4703.1085

Chen, D., Lian, T., Fu, C., Cane, M. A., Tang, Y., Murtugudde, R., et al. (2015). Strong influence of westerly wind bursts on El Niño diversity. *Nature Geoscience*, *8*(5), 339–345. https://doi.org/10.1038/ngeo2399

Chen, H. C., & Jin, F. F. (2020). Fundamental behavior of ENSO phase locking. *Journal of Climate*, *33*(5), 1953–1968. https://doi.org/10.1175/jcli-d-19-0264.1

Chiodi, A. M., Harrison, D. E., & Vecchi, G. A. (2014). Subseasonal atmospheric variability and El Niño waveguide warming: Observed effects of the Madden–Julian oscillation and westerly wind events. *Journal of Climate*, *27*(10), 3619–3642. https://doi.org/10.1175/jcli-d-13-00547.1

Copernicus Climate Change Service, Climate Data Store. (2021). ORAS5 global ocean reanalysis monthly data from 1958 to present [Dataset]. *Copernicus Climate Change Service (C3S) Climate Data Store (CDS)*. https://doi.org/10.24381/cds.67e8eeb7

Dewitte, B., Thual, S., Yeh, S. W., An, S. I., Moon, B. K., & Giese, B. S. (2009). Low-frequency variability of temperature in the vicinity of the equatorial Pacific thermocline in SODA: Role of equatorial wave dynamics and ENSO asymmetry. *Journal of Climate*, *22*(21), 5783–5795. https://doi.org/10.1175/2009jcli2764.1

Fedorov, A. V., Hu, S., Lengaigne, M., & Guilyardi, E. (2015). The impact of westerly wind bursts and ocean initial state on the development, and diversity of El Niño events. *Climate Dynamics*, *44*(5–6), 1381–1401. https://doi.org/10.1007/s00382-014-2126-4

Graham, N. E., & Barnett, T. P. (1987). Sea surface temperature, surface wind divergence, and convection over tropical oceans. *Science*, *238*(4827), 657–659. https://doi.org/10.1126/science.238.4827.657

Harrison, D. E., & Giese, B. S. (1991). Episodes of surface westerly winds as observed from islands in the western tropical Pacific. *Journal of Geophysical Research*, *96*(S01), 3221–3237. https://doi.org/10.1029/90jc01775

Harrison, D. E., & Vecchi, G. A. (1997). Westerly wind events in the tropical Pacific, 1986–95. *Journal of Climate*, *10*(12), 3131–3156. https://doi.org/10.1175/1520-0442(1997)010<3131:wweitt>2.0.co;2

Hartten, L. M. (1996). Synoptic settings of westerly wind bursts. *Journal of Geophysical Research*, *101*(D12), 16997–17019. https://doi.org/10.1029/96jd00030

Hersbach, H., Bell, B., Berrisford, P., Biavati, G., Horányi, A., Muñoz Sabater, J., et al. (2023). ERA5 monthly averaged data on single levels from 1940 to present [Dataset]. *Copernicus Climate Change Service (C3S) Climate Data Store (CDS)*. https://doi.org/10.24381/cds.f17050d7

Hersbach, H., Bell, B., Berrisford, P., Hirahara, S., Horanyi, A., Muñoz-Sabater, J., et al. (2020). The ERA5 global reanalysis. *Quarterly Journal of the Royal Meteorological Society*, *146*(730), 1999–2049. https://doi.org/10.1002/qj.3803

Horii, T., & Hanawa, K. (2004). A relationship between timing of El Niño onset and subsequent evolution. *Geophysical Research Letters*, *31*(6). https://doi.org/10.1029/2003gl019239

Hu, S., Zhang, W., Watanabe, M., Jiang, F., Jin, F. F., & Chen, H. C. (2024). Equatorial western–central pacific SST responsible for the north pacific oscillation–ENSO Sequence. *Journal of Climate*, *37*(11), 3191–3204. https://doi.org/10.1175/jcli-d-23-0434.1

Jiang, F., Zhang, W., Jin, F. F., Stuecker, M. F., Timmermann, A., McPhaden, M. J., et al. (2023). Resolving the tropical Pacific/Atlantic interaction conundrum. *Geophysical Research Letters*, *50*(13), e2023GL103777. https://doi.org/10.1029/2023gl103777

Jin, F. F. (1997). An equatorial ocean recharge paradigm for ENSO. Part I: Conceptual model. *Journal of the Atmospheric Sciences*, *54*(7), 811–829. https://doi.org/10.1175/1520-0469(1997)054<0811:aeorpf>2.0.co;2

Jin, F. F., & An, S. I. (1999). Thermocline and zonal advective feedbacks within the equatorial ocean recharge oscillator model for ENSO. *Geophysical Research Letters*, *26*(19), 2989–2992. https://doi.org/10.1029/1999gl002297

Kleeman, R., & Moore, A. M. (1997). A theory for the limitation of ENSO predictability due to stochastic atmospheric transients. *Journal of the Atmospheric Sciences*, *54*(6), 753–767. https://doi.org/10.1175/1520-0469(1997)054<0753:atftlo>2.0.co;2

Lai, A. W. C., Herzog, M., & Graf, H. F. (2015). Two key parameters for the El Niño continuum: Zonal wind anomalies and western pacific subsurface potential temperature. *Climate Dynamics*, *45*(11), 3461–3480. https://doi.org/10.1007/s00382-015-2550-0

Lee, S. K., DiNezio, P. N., Chung, E. S., Yeh, S. W., Wittenberg, A. T., & Wang, C. (2014). Spring persistence, transition, and resurgence of El Niño. *Geophysical Research Letters*, *41*(23), 8578–8585. https://doi.org/10.1002/2014gl062484

Lengaigne, M., Boulanger, J. P., Menkes, C., Madec, G., Delecluse, P., Guilyardi, E., & Slingo, J. (2003). The March 1997 westerly wind event and the onset of the 1997/98 El Niño: Understanding the role of the atmospheric response. *Journal of Climate*, *16*(20), 3330–3343. https://doi.org/10.1175/1520-0442(2003)016<3330:tmwwea>2.0.co;2

Lengaigne, M., Guilyardi, E., Boulanger, J. P., Menkes, C., Delecluse, P., Inness, P., et al. (2004). Triggering of El Niño by westerly wind events in a coupled general circulation model. *Climate Dynamics*, *23*(6), 601–620. https://doi.org/10.1007/s00382-004-0457-2

Liebmann, B., & Smith, C. A. (1996). Description of a complete (interpolated) outgoing longwave radiation dataset. *Bulletin of the American Meteorological Society*, *77*, 1275–1277.

Lopez, H., Lee, S. K., Kim, D., Wittenberg, A. T., & Yeh, S. W. (2022). Projections of faster onset and slower decay of El Niño in the 21st century. *Nature Communications*, *13*(1), 1915. https://doi.org/10.1038/s41467-022-29519-7

McPhaden, M. J. (1999). Genesis and evolution of the 1997-98 El Niño. *Science*, *283*(5404), 950–954. https://doi.org/10.1126/science.283.5404.950

McPhaden, M. J., & Yu, X. (1999). Equatorial waves and the 1997–98 El Niño. *Geophysical Research Letters*, *26*(19), 2961–2964. https://doi.org/10.1029/1999gl004901

McPhaden, M. J., Zebiak, S. E., & Glantz, M. H. (2006). ENSO as an integrating concept in earth science. *Science*, *314*(5806), 1740–1745. https://doi.org/10.1126/science.1132588

Meinen, C. S., & McPhaden, M. J. (2000). Observations of warm water volume changes in the equatorial Pacific and their relationship to El Niño and La Niña. *Journal of Climate*, *13*(20), 3551–3559. https://doi.org/10.1175/1520-0442(2000)013<3551:oowwvc>2.0.co;2

Palmer, T. N., & Mansfield, D. A. (1984). Response of two atmospheric general circulation models to sea-surface temperature anomalies in the tropical east and west Pacific. *Nature*, *310*(5977), 483–485. https://doi.org/10.1038/310483a0

Reynolds, R. W., Smith, T. M., Liu, C., Chelton, D. B., Casey, K. S., & Schlax, M. G. (2007). Daily high-resolution-blended analyses for sea surface temperature. *Journal of Climate*, *20*(22), 5473–5496. https://doi.org/10.1175/2007jcli1824.1

Seiki, A., & Takayabu, Y. N. (2007). Westerly wind bursts and their relationship with intraseasonal variations and ENSO. Part I: Statistics. *Monthly Weather Review*, *135*(10), 3325–3345. https://doi.org/10.1175/mwr3477.1

Suarez, M. J., & Schopf, P. S. (1988). A delayed action oscillator for ENSO. *Journal of the Atmospheric Sciences*, *45*(21), 3283–3287. https://doi.org/10.1175/1520-0469(1988)045<3283:adaofe>2.0.co;2

Tatebe, H., Ogura, T., Nitta, T., Komuro, Y., Ogochi, K., Takemura, T., et al. (2019). Description and basic evaluation of simulated mean state, internal variability, and climate sensitivity in MIROC6. *Geoscientific Model Development*, *12*(7), 2727–2765. https://doi.org/10.5194/gmd-12-2727-2019

Timmermann, A., An, S. I., Kug, J. S., Jin, F. F., Cai, W., Capotondi, A., et al. (2018). El Niño–southern oscillation complexity. *Nature*, *559*(7715), 535–545. https://doi.org/10.1038/s41586-018-0252-6

Tziperman, E., & Yu, L. (2007). Quantifying the dependence of westerly wind bursts on the large-scale tropical Pacific SST. *Journal of Climate*, *20*(12), 2760–2768. https://doi.org/10.1175/jcli4138a.1

Wallace, J. M., Rasmusson, E. M., Mitchell, T. P., Kousky, V. E., Sarachik, E. S., & von, S. H. (1998). On the structure and evolution of ENSO-related climate variability in the tropical Pacific: Lessons from TOGA. *Journal of Geophysical Research*, *103*(C7), 14241–14259. https://doi.org/10.1029/97jc02905

Wu, X., Okumura, Y. M., & DiNezio, P. N. (2021). Predictability of El Niño duration based on the onset timing. *Journal of Climate*, *34*(4), 1351–1366. https://doi.org/10.1175/jcli-d-19-0963.1

Wyrtki, K. (1975). El Niño—The dynamic response of the equatorial pacific oceanto atmospheric forcing. *Journal of Physical Oceanography*, *5*(4), 572–584. https://doi.org/10.1175/1520-0485(1975)005<0572:entdro>2.0.co;2

Wyrtki, K. (1985). Water displacements in the pacific and the genesis of El Niño cycles. *Journal of Geophysical Research*, *90*(C4), 7129–7132. https://doi.org/10.1029/jc090ic04p07129

Xu, J., & Chan, J. C. (2001). The role of the Asian–Australian monsoon system in the onset time of El Niño events. *Journal of Climate*, *14*(3), 418–433. https://doi.org/10.1175/1520-0442(2001)014<0418:trotaa>2.0.co;2

Xuan, Z., Zhang, W., Jiang, F., & Jin, F. F. (2022). Effective ENSO amplitude forecasts based on oceanic and atmospheric preconditions. *Journal of Climate*, *35*(11), 3279–3291. https://doi.org/10.1175/jcli-d-21-0383.1

Xuan, Z., Zhang, W., Jiang, F., Stuecker, M. F., & Jin, F. F. (2024). Seasonal-varying characteristics of tropical Pacific westerly wind bursts during El Niño due to annual cycle modulation. *Climate Dynamics*, *62*(1), 299–314. https://doi.org/10.1007/s00382-023-06907-3

Yuan, X., Jin, F. F., & Zhang, W. (2020). A concise and effective expression relating subsurface temperature to the thermocline in the equatorial Pacific. *Geophysical Research Letters*, *47*(15), e2020GL087848. https://doi.org/10.1029/2020gl087848

Zebiak, S. E. (1989). Oceanic heat content variability and El Niño cycles. *Journal of Physical Oceanography*, *19*(4), 475–486. https://doi.org/10.1175/1520-0485(1989)019<0475:ohcvae>2.0.co;2

Zhang, W., Li, S., Jin, F. F., Xie, R., Liu, C., Stuecker, M. F., & Xue, A. (2019). ENSO regime changes responsible for decadal phase relationship variations between ENSO sea surface temperature and warm water volume. *Geophysical Research Letters*, *46*(13), 7546–7553. https://doi.org/10.1029/2019gl082943

Zhao, S., Jin, F. F., Long, X., & Cane, M. A. (2021). On the breakdown of ENSO's relationship with thermocline depth in the central-equatorial Pacific. *Geophysical Research Letters*, *48*(9), e2020GL092335. https://doi.org/10.1029/2020gl092335

Zuo, H., Balmaseda, M. A., Mogensen, K., Tietsche, S., & Mayer, M. (2019). The ECMWF operational ensemble reanalysis–analysis system for ocean and sea ice: A description of the system and assessment [dataset]. *Ocean Science*, *15*(3), 779–808. https://doi.org/10.5194/os-15-779-2019

References From the Supporting Information

Chen, H. C., & Jin, F. F. (2022). Dynamics of ENSO phase–locking and its biases in climate models. *Geophysical Research Letters*, *49*(3), e2021GL097603. https://doi.org/10.1029/2021gl097603

Levine, A. F., & McPhaden, M. J. (2016). How the July 2014 easterly wind burst gave the 2015–2016 El Niño a head start. *Geophysical Research Letters*, *43*(12), 6503–6510. https://doi.org/10.1002/2016gl069204